Observation of pulsating dissipative solitons in a Mamyshev oscillator

Bo Cao,[1] Kangjun Zhao,[1] Chenxin Gao,[1] Xiaosheng Xiao,[2] Chengying Bao,[1,*] and Changxi Yang[1,†]

[1]*State Key Laboratory of Precision Measurement Technology and Instruments, Department of Precision Instruments, Tsinghua University, Beijing 100084, China*

[2]*State Key Laboratory of Information Photonics and Optical Communications, School of Electronic Engineering, Beijing University of Posts and Telecommunications, Beijing 100876, China*

(Received 26 May 2022; accepted 29 July 2022; published 18 August 2022)

Dissipative solitons (DSs) widely exist in optical systems and mode-locked fiber lasers provide a versatile playground to study their dynamics. Recently, Mamyshev oscillators (MOs), which rely upon a pair of narrow filters with offset passing frequencies, have emerged as a new type of femtosecond fiber lasers. Besides creating high-energy broadband DSs, MOs have been predicted to support periodically pulsating DSs whose observation remains elusive. Here, we present a comprehensive experimental and numerical investigation of pulsating DSs in an ytterbium MO. By reducing the filter separation, we observe pulsation in both single-pulse and DS molecule states. The output pulse energy can vary as large as 40 times in our MO. Single-shot spectra measured by the dispersive Fourier transform method further enables the observation of spectral bandwidth breathing and soliton explosion in the pulsation. In addition, pulsation lasting 9 round trips and even a chaotic pulsation state are observed. Numerical simulations based on a lumped vector model qualitatively agree with our observation. Our results enrich pulsating DS dynamics and reveal the impact of filter separation on the stability of MOs.

DOI: 10.1103/PhysRevA.106.023519

I. INTRODUCTION

Optical dissipative solitons (DSs) are a subject of intense theoretical and experimental studies [1]. The stability endowed by stable propagation of DSs makes them invaluable for applications spanning from nonlinear microscopy [2] to precise timing dissemination [3] to optical frequency combs [4]. Similar to breathers in conservative systems [5,6], DSs can undergo periodic variation besides stable propagation in dissipative systems. For instance, both the cubic-quintic Ginzburg-Landau equation (CGLE, governing DSs in mode-locked lasers [7–11]) and the Lugiato-Lefever equation (governing DSs in coherently pumped microcavities [4,12,13]) admit pulsating or breathing DSs. The ability to carefully tailor laser parameters including net dispersion, filter profile, active gain and loss, makes mode-locked fiber lasers a versatile platform to study pulsating DSs. The CGLE averages the DS propagation within a single round trip. When considering the round trip nature of lasers, pulsation of DSs manifests as period multiplication (period-N pulsation means DSs only repeat after N round trips) in mode-locked fiber lasers [14–17].

Limited by the bandwidth of electronic digitizers, early reports on DS pulsation in mode-locked lasers mainly focused on pulse energy variation [14–16] and it was quite challenging to measure the pulsation of other parameters. With the emergence of the dispersive Fourier transform (DFT) method [18], single-shot spectra during pulsation have been measured recently [19–23]. These measurements reveal that pulsating DSs can be associated with strong spectral breathing [21] or even be invisible if only pulse energy is measured [19].

To date, pulsating DSs have been observed in fiber lasers mode-locked by material-based saturable absorbers [19,20,24] and by nonlinear polarization rotation (NPR) [15–17,21]. Recently, a new saturable absorption mechanism based on the Mamyshev regenerators [25] has been leveraged for DS formation in fiber lasers [26–31]. This effective saturable absorber relies upon spectral broadening induced by self-phase modulation (SPM) and a pair of filters with offset transmission frequencies [25]. Thus, a high-power optical field will pass the filter pair with higher transmission than that of a low-power field, resulting in an effective saturable absorber [32–34]. Mode-locked fiber lasers based on this mechanism, referred to as Mamyshev oscillators (MOs), show great prospects in reaching high output pulse energy and broad bandwidth [26,27,29,35]. The unique architecture of MOs also makes them a new playground to study DS dynamics (for example, filter separation adds a new freedom to control DS dynamics). Indeed, pulsating solitons have also been predicted in concatenated Mamyshev regenerators (termed as limited cycles therein) [33,36], which effectively have the same underlying physics as MOs.

Here, we report experimental and numerical observation of pulsating DSs in a MO operating around 1030 nm. Pulsating DSs are observed by controlling the filter separation. Single-shot spectra of these pulsating DSs are also measured by the DFT method, which indicate that our MO admits various pulsation dynamics. Spectral breathing associated with pulse-energy pulsation occurs for both a single-pulse state or a DS molecule state in period-2 pulsation states. In the single-pulse

*cbao@tsinghua.edu.cn
†cxyang@tsinghua.edu.cn

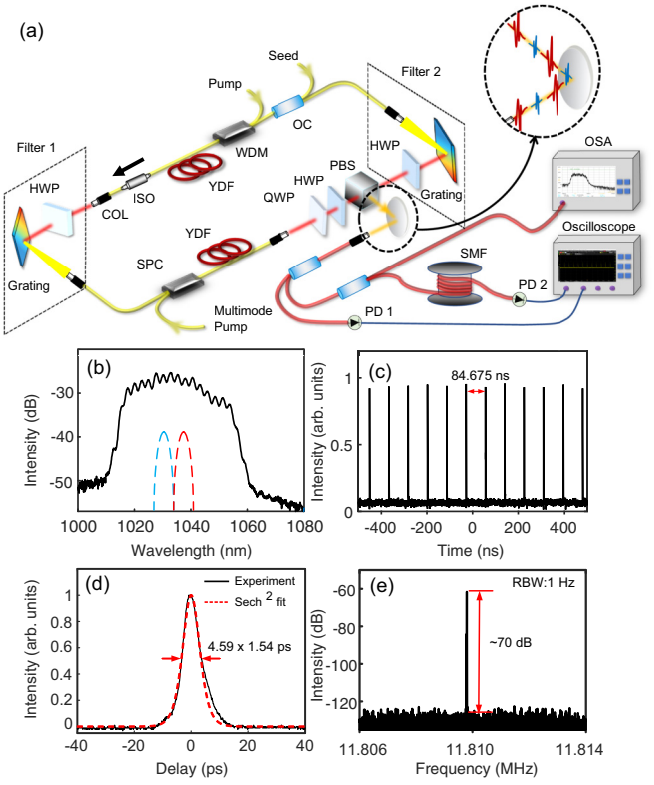

FIG. 1. Experimental setup and a stable laser output. (a) Schematic of the Mamyshev oscillator (MO) and the measurement system. The top inset illustrates a train of dissipative solitons in pulsation. OC, optical coupler; WDM, wavelength division multiplexer; COL, collimator; ISO, isolator; HWP, half-wave plate; QWP, quarter-wave plate; PBS, polatization beam splitter; SMF, single-mode fiber; SPC, signal-pump combiner; PD, photodetector. (b) Optical spectrum of the MO output with a filter separation of 7 nm. The dashed blue and the dashed red curves correspond to the transmission of the filters. (c) Pulse train of the MO output. (d) Autocorrelation trace, showing a pulse width of 4.6 ps. (e) Radio-frequency spectrum.

state, pulsating DSs whose output energy varies as large as 40 times during pulsation are observed. Period-3 pulsation is observed for two wide-spaced DSs pulsating in different ways. Intermittent and relatively mild soliton explosion [20,22,37–39] is also observed in this state. In addition to these short-period pulsations, pulsation lasting a relatively long period (e.g., 9 round trips) and even chaotic pulsation (no regular period) also exist in the MO. Our experimental observation is organized in the order of pulsation period in the following. Numerical simulations based on a lumped model including the polarization dynamics are in reasonably qualitative agreement with the experimental observation. Our observation not only adds to the possible DS states in MOs but also aids in the design of MOs.

II. LASER DESIGN AND STABLE OPERATION

The scheme of the experimental setup is shown in Fig. 1(a). The laser cavity consists of two Mamyshev regenerators. The upper arm comprises a 2-m-core pumped Yb fiber with a small core diameter of 6 μm so as to enhance the nonlinearity. Thus, a 976-nm single-mode pump is sufficient to amplify the seeding pulses to pass filter 2 via SPM-induced spectral broadening [see Fig. 1(a)]. For the second arm, a 1.5-m double-cladding Yb-fiber (LMA-10/125-YDF, Nufern) is pumped by a 976-nm multimode pump so that a higher output power is possible. All the remaining passive fibers in the cavity are HI1060 fibers. An isolator is used to ensure unidirectional propagation. To realize offset filtering, a pair of 600 lines/mm reflective diffraction gratings (GR13-0610, Thorlabs) are used to form two filters whose passing band can be adjusted by the grating orientation and the collimator position [dotted squares in Fig. 1(a)] [27]. Two half-wave plates are placed before the gratings to maximize the diffraction efficiency. The filter bandwidth is measured to be ∼2 nm. The other wave plates and a polarizing beam splitter (PBS) are used to create a NPR-like transmission in the cavity that can assist initialization of the mode-locking. Note that the wave plates can be adjusted over a wide range (in some cases 360° for the QWP) without losing mode-locking after pulses generated, which elucidates the effect of Mamyshev regenerators on stabilizing the mode-locked pulses. However, the observed pulsation dynamics depends on the NPR strongly. Indeed, NPR adds a freedom and enriches the observed pulsating DS dynamics in experiments.

The pulses are sampled by the PBS as the output. The pulse train is detected by a 5-GHz photodetector (PD 1) and a 12-GHz photodetector (PD 2) and digitized by a real-time oscilloscope (Keysight DSOS804A) with an effective bandwidth of 4 GHz [see Fig. 1(a)]. The limited bandwidth hinders us from measuring the temporal pulsation details directly. The averaged optical spectra are recorded by an optical spectrum analyzer (OSA, Agilent 86142B) with a resolution of 0.06 nm. The DFT path includes a 12-km single-mode fiber (SMF), corresponding to a net group delay dispersion of ∼360 ps/nm around 1030 nm. The resolution of single-shot DFT spectra is estimated to be 0.58 nm [18].

To initiate mode-locking in the MO, we inject seed pulses from a home-built all normal dispersion fiber laser [40] into the MO. The seeding pulse has a ∼10-nm bandwidth that covers the filter separation. Filter 1 is set to 1030 nm while filter 2 is adjusted between 1034 and 1038 nm. When the single-mode pump and the multimode pump are adjusted to 400 mW and 1.1 W, respectively, stable mode-locking can be achieved by adjusting the waveplates. Once initiated, the mode-locked pulse circulates stably in the MO after blocking the seed laser. By increasing the filter separation to 7 nm and increasing the pump (multimode pump, the same below) power to 1.3 W after starting mode-locking [41], we get a stable mode-locking state whose characteristics are depicted in Figs. 1(b)–1(e). The pulse spectrum spans about 50 nm at the −20-dB level and the mode-locked pulse train has a repetition rate of 11.81 MHz. This bandwidth is relatively narrow compared to other reported MOs [27,29], as we focused on studying the pulsation dynamics and the MO was not optimized for broadband operation. Moreover, the spectrum exhibits modulation. This modulation may be a feature of SPM-based spectral broadening or a secondary small pulse spaced by about 1.5 ps away from the main pulse. The potential close-spaced secondary pulse is not observed in the

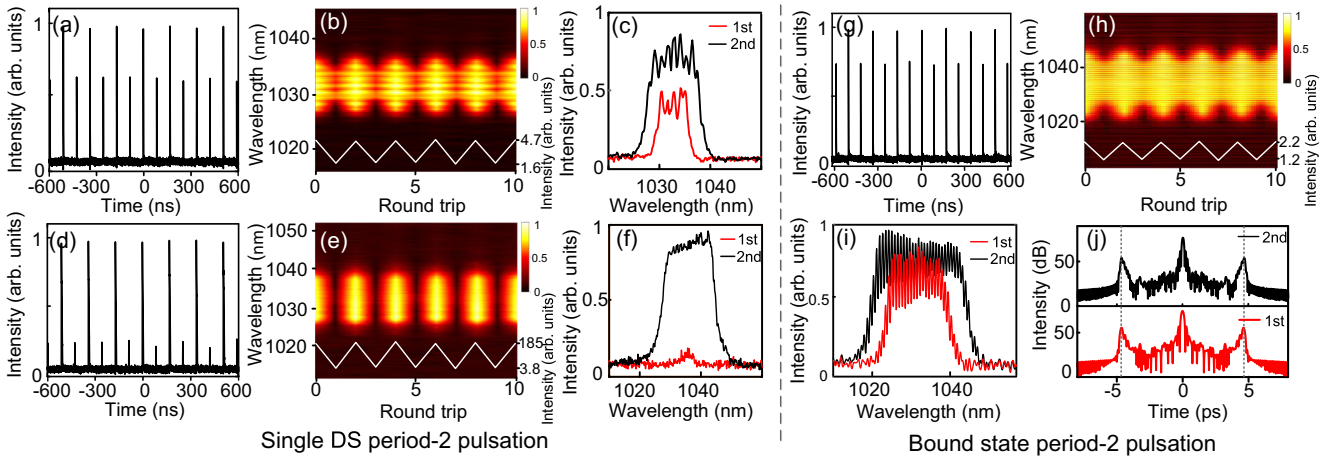

FIG. 2. Single DS and DS molecule period-2 pulsation. (a) and (d) Pulsation pulse trains of the two typical states. (b) and (e) DFT-measured single-shot spectra corresponding to panels (a) and (d), respectively. The white curves are the integrated spectral power for the pulsating DS. (c) and (f) Single-shot spectra in 2 successive round trips. (g) Pulsating pulse train of a DS molecule. (h) Single-shot spectra of the pulsation state. (i) Spectra of 2 successive round trips. The spectra show modulation due to the interference between two closely spaced pulses. (j) Fourier transform of panel (i). Peaks at 4.65 ps illustrate the pulse separation of the DS molecule.

autocorrelation measurement, as the pulse is highly chirped and as long as 4.6 ps [Fig. 1(d)]. Furthermore, the modulation contrast suggests the secondary pulse may only have a peak power $1/3$ that of the main pulse. We did not dechirp the pulse in our experiment (dechirping may also help to reveal the weak pulse [42]), since we did not aim at generating ultrashort pulses from stable states. Nevertheless, it has been shown the pulse from MOs can be dechirped with high pulse quality [27,29]. The radio-frequency (rf) spectrum of the pulse train exhibits a signal-to-noise ratio of ∼70 dB with a resolution bandwidth of 1 Hz [see Fig. 1(e)], showing a good stability in this state.

III. EXPERIMENTAL RESULTS

A. Period-2 pulsation

The laser tends to operate in the stable regime when the filter separation is relatively large. When decreasing the filter separation to 4 nm by tuning filter 2 to ∼1034 nm under a pump power of 1.1 W, pulsating DSs can be observed frequently in the MO. This is consistent with the prediction in Ref. [33]. The operation regime of the MO can be adjusted by the polarization dynamics. Various pulsation states can be accessed by rotating the wave plates under this relatively narrow filter separation. This also enables a comprehensive study of pulsation dynamics in our MO. We present two typical examples of single-pulse period-2 pulsation states in Figs. 2(a)–2(f). A pulse train is plotted in Fig. 2(a), showing that pulses in successive round trips have significant intensity change. Figure 2(b) shows the periodic change of the DFT-measured single-shot spectra in 11 round trips; pulse energy derived by integrating the single-shot spectra power also exhibits period-doubling. To show more details of the pulsation, spectra of 2 successive round trips are shown in Fig. 2(c). These two spectra show variations in 3-dB bandwidth (changing between 5 and 11 nm), spectral fringe features, and average power. The large spectral bandwidth breathing can be attributed to the different spectral broadenings in the Mamyshev regenerators when the pulse energy changes in the pulsation. Note that the narrower spectrum still covers the two filters (4 nm separated). Thus, it can be regenerated to retain mode-locking.

By rotating the wave plates, the output pulse energy variation can be very large in some cases. Figures 2(d)–2(f) show an extreme example, where one of the output DSs can be very weak. The output pulse energy change (defined as the ratio between the strong and the weak one) is as large as 40 times within one pulsation cycle by integrating the single-shot spectra (note that the time domain measurement does not show such a high ratio as the detector is saturated for the strong pulse in order to measure the weak one). This corresponds to a very large pulse energy variation during pulsation in mode-locked lasers. As a caveat, the PBS output port is a nonlinear output port and the intracavity pulse energy may not change as much as the output (see also simulations below). In other words, the large output energy variation between 2 successive round trips may arise from significant nonlinear polarization rotation in 2 round trips. This may help the intracavity pulse to retain an energy level required to keep consistent spectral broadening in the MO. Therefore, the large output energy variation may not provide direct experimental evidence for the theoretically predicted extreme pulsation with energy variation exceeding 2 orders of magnitude yet [43]. Nevertheless, the intracavity dynamics is highly nonlinear and polarization rotation impacts both spectral broadening along two orthogonal directions and gain competition between them. Hence, it is likely both polarization and intracavity energy change in pulsation.

By increasing the pump power to 1.2 W, a pulsation state comprising two bounded DSs (i.e., a DS molecule [44]) can be obtained by rotating the wave plates. Figure 2(g) shows a pulse train measured without DFT, which indicates period-2 pulsation. The associated single-shot spectra are presented

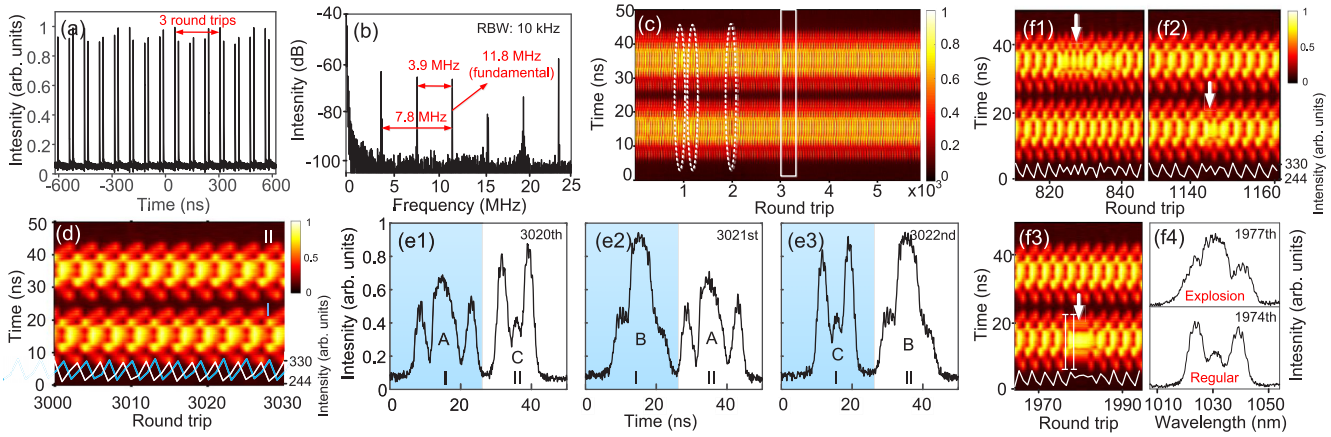

FIG. 3. Period-3 pulsation and explosion for two wide-spaced DSs. (a) A pulse train showing pulse energy period-3 pulsation. (b) The rf spectrum of the pulse train exhibiting multiple rf tones at harmonics of 1/3 of the fundamental repetition rate (11.8 MHz). (c) Single-shot spectra in 6001 round trips. Note that the y axis of this panel is labeled as time rather than wavelength derived from DFT (i.e., time to wavelength mapping). This is because the two pulses are plotted with increasing time but they share the same wavelength. (d) Zoom-in of the data marked by the rectangular shape in panel (c) showing a regular period-3 pulsation. The light blue and white curves are the pulse energy change for DS I and DS II, respectively. (e1)–(e3) Spectra of the pulsating dissipative solitons within a single pulsation period. DS I and DS II both undergo spectra A, B, and C in pulsation, but experience them in different orders. (f1)–(f3) Zoom-in of the data marked by the ellipse shape in panel (c). The single-shot spectra show abrupt spectral distortion in soliton explosion, as indicated by the arrows. The white curves show the integrated spectral power for the DS in explosion. (f4) Two typical single-shot spectra from panel (f3), one in regular pulsation (1974th round trip) and the other in explosion (1977th round trip).

in Fig. 2(h). Stretching and compression of the spectra are evident and the weak pulse has an energy about half that of the strong one.

To compare the pulsating spectra, spectra of 2 consecutive round trips are shown in Fig. 2(i). The measured spectra exhibit evident spectral modulation, which arises from the interference between two closely spaced DSs [45]. The contrast of the spectral fringe is lower than unity due to the finite resolution of the DFT method. Similar to the single soliton pulsation in Fig. 2, the 3-dB bandwidth of the soliton molecule spectra changes from 25 to 16 nm in the pulsation. Fourier transform of the single-shot spectra in Fig. 2(i) is plotted in Fig. 2(j). Peaks at nonzero time delay can be observed and they indicate that the two pulsating DSs are separated by 4.65 ps. This separation remains the same during pulsation, which differs from the vibrating solitons whose pulse separation changes periodically [46–48].

B. Period-3 pulsation and soliton explosion

For higher pump power (e.g., exceeding 1.2 W), a multi-DS state occurs frequently. We also observe pulsation in a two-DS state with the pulses widely spaced. Figure 3(a) plots the nonuniform pulse train in the time domain. This state shows period-3 pulsation instead of period-2 pulsation. As a result, the rf spectrum of the pulse train shows rf tones at the harmonics of 11.8 MHz/3 besides the fundamental 11.8 MHz [Fig. 3(b)].

Single-shot spectra over 6001 round trips are presented in Fig. 3(c). We first zoom-in the data of 31 round trips around the 3000th round trip in Fig. 3(d) [rectangular shaped region in Fig. 3(c)]. Although the two DSs both have period-3 pulsation, they pulsate in two ways. The single-shot spectra within 3 successive round trips are depicted in Fig. 3(e1)–3(e3). DSs show three different spectral shapes marked as A, B, and C. DS I pulsates in a route as A → B → C, while DS II pulsates as C → A → B . In other words, both DSs exhibit three spectral states in pulsation, but experience them in an asynchronous way. This also corroborates the pulse energy change delay in Fig. 3(d). Such a delayed spectral evolution can reduce the total pulse energy change more than a synchronized spectral evolution.

Besides the periodic pulsation, there are some round trips where the DSs experience soliton explosion [see ellipse regions in Fig. 3(c)]. These soliton explosions associated abrupt spectral distortion occur randomly, and details of the explosion are indicated by arrows in Figs. 3(f1)–3(f3). Typically, DSs recover to a steady state in soliton explosion [37,38], and soliton explosion for pulsating DSs has only been recently reported for a NPR mode-locked fiber laser [22] and carbon-nanotube mode-locked fiber lasers [20,39]. Here, soliton explosion for pulsating DSs is observed in a MO. Different from collapsing into chaotic and wide spectra as shown in Ref. [22], spectral bandwidth does not change too much, but the central part becomes stronger in our observed explosion [see Fig. 3(f4)]. The relatively mild spectral distortion may be attributed to the strong shaping effect on pulses of Mamyshev regenerators; extreme explosion may not survive in concatenated offset frequency filtering. The explosion lasts for about 5 round trips (∼400 ns) which is much smaller than the ∼20-μs explosion timescale reported in Ref. [22]. The pump power for this state (1.3 W) is higher than the mode-locking threshold (1.1 W) and we believe that strong nonlinearity is essential to the observation of explosion in pulsation in our MO. As an aside, when one of the DSs undergoes the explosion, the other one pulsates regularly; this suggests that the interaction is relatively weak for these two widely spaced DSs.

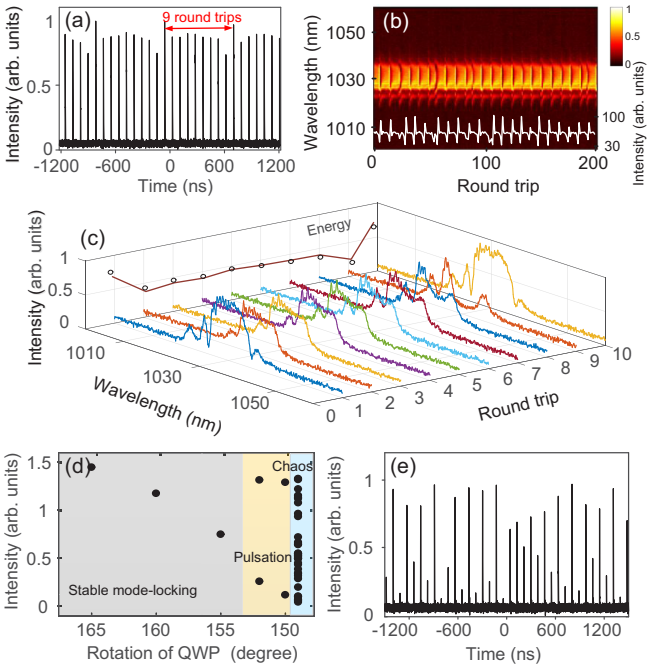

FIG. 4. Long-period pulsation and bifurcation to a chaotic state. (a) A pulse train showing period-9 pulsation. (b) Single-shot spectra of the period-9 pulsation state. The white line shows the integrated spectral power during pulsation. (c) Details of the spectral evolution within one pulsation period. (d) Pulse energy bifurcation diagram when rotating the quarter-wave plate. (e) Pulse train in a chaotic pulsation state under a wave-plate orientation of 148°.

C. Long-period and chaotic pulsation

In addition to the short-period pulsation shown above, pulsation with a relatively long period can also be possible in fiber lasers. For example, long-period pulsation (up to 170 round trips) associated with spectral bandwidth breathing has been reported in NPR mode-locked lasers [21]. This type of long-period pulsation can also be observed by careful control of the polarization state in our MO under a pump power of 1.15 W. Figure 4(a) plots the pulse train of an observed period-9 pulsation. Figure 4(b) records the spectral evolution of 201 round trips, where we also notice abrupt spectral breathing during long-period pulsation. The spectrum broadens about 1.5 times compared to the narrowest one (from 10 to 15 nm for a 3-dB bandwidth), which creates significant spectral content in the wings of the spectrum. We plot the spectral evolution within one pulsation period in Fig. 4(c). The figure shows that the energy near the spectral center gradually decreases and transfers to the spectral wings during pulsation and this evolution repeats in 9 round trips. Note that the periodicity is not very robust in this long-period pulsation, which can be seen from the power variation in Fig. 4(b).

Beyond this long-period pulsation, the chaotic state can also be realized in our MO. The route towards the chaotic state can be controlled by fine-tuning of the wave plates [for example, QWP in Fig. 1(a)]. When the angle of the quarter-wave plate is about 165°, the MO operates in the stable state [see Fig. 4(d)]. The pulse energy decreases as the wave plate rotates counterclockwise. Period-2 pulsation appears at an angle of 153°. Further tuning of the quarter-wave plates leads to a chaotic state [Fig. 4(e)]. The pulse train can no longer repeat itself in this state. Further experiments show that all DS forms (e.g., single-DS, multi-DS, and DS molecule) can bifurcate from stable operation to multiperiod pulsating and even to chaos, which suggests that chaotic pulsation is a ubiquitous phenomenon in our MO. The observed route towards chaotic pulsation is quite different from the route towards chaos controlled by dispersion predicted in Ref. [36].

IV. NUMERICAL SIMULATIONS

A. Period-2 pulsation in simulations

To have a deeper understanding of our experimental observations, we use a lumped model to simulate the pulsating DS dynamics in the MO. Since polarization dynamics is important in our experiment, we use coupled generalized nonlinear Schrödinger equations to simulate pulse propagation in the fibers and the Jones matrix to model the wave plates and PBS. Details of the simulations are provided in the Appendix, which also include parameters used in the simulations. Consistent with experiments, small filter separation can lead to pulsation in simulations. Figure 5(a) shows an example of generating pulsating DSs by reducing the filter separation from 6 to 3 nm from a stable mode-locking state. In agreement with the experiment, the pulsating DSs are also associated with spectral breathing, with the 3-dB bandwidth varying from 10 to 12 nm in the pulsation [see inset in Fig. 5(a)]. In another case, pulsation can also be attained from stable mode-locking by adjusting the wave plates with the filter separation and fixing the bandwidth at 3 and 0.8 nm, respectively [see Fig. 5(b)].

The pulse energy change during pulsation can be adjusted by increasing the gain of the active fibers and rotating the wave plates in simulations (see Table II in the Appendix). Figures 5(c) and 5(d) show temporal and spectral dynamics within 2 successive round trips of a pulsation state with a relatively large pulse energy change. Both the pulse energy and the duration quickly increase during propagation in the gain fiber. Then the duration continues to grow in the single-mode fiber and the chirped pulse is shortened by the filter before entering YDF2 and SMF3 (i.e., another arm of the MO). The pulse has different intensity at the end of YDF1 in 2 round trips [see white line in Fig. 5(c)], which leads to the difference of spectral broadening in Fig. 5(d). Figure 5(e) shows the normalized spectra before filter 2 in 2 successive round trips. The spectra feature fringes, implying the spectral broadening is dominated by SPM. And the center of the output pulse also changes slightly (∼0.275 ps) in pulsation, similar to a moving (creeping), pulsating soliton [10] (see more details in the Appendix). The insets of Fig. 5(d) show the spectra right after filter 1, whose relative spectral power can be determined from the colorbar.

The simulated pulse energy change is 3.3 times in Figs. 5(c)–5(e). Although this is still much smaller than the 40 times observed in Fig. 2(e), we believe a larger energy change can be possible by further exploration of the parameters. Simulation verifies that polarization effects and using the PBS as the output port are important to have a relatively

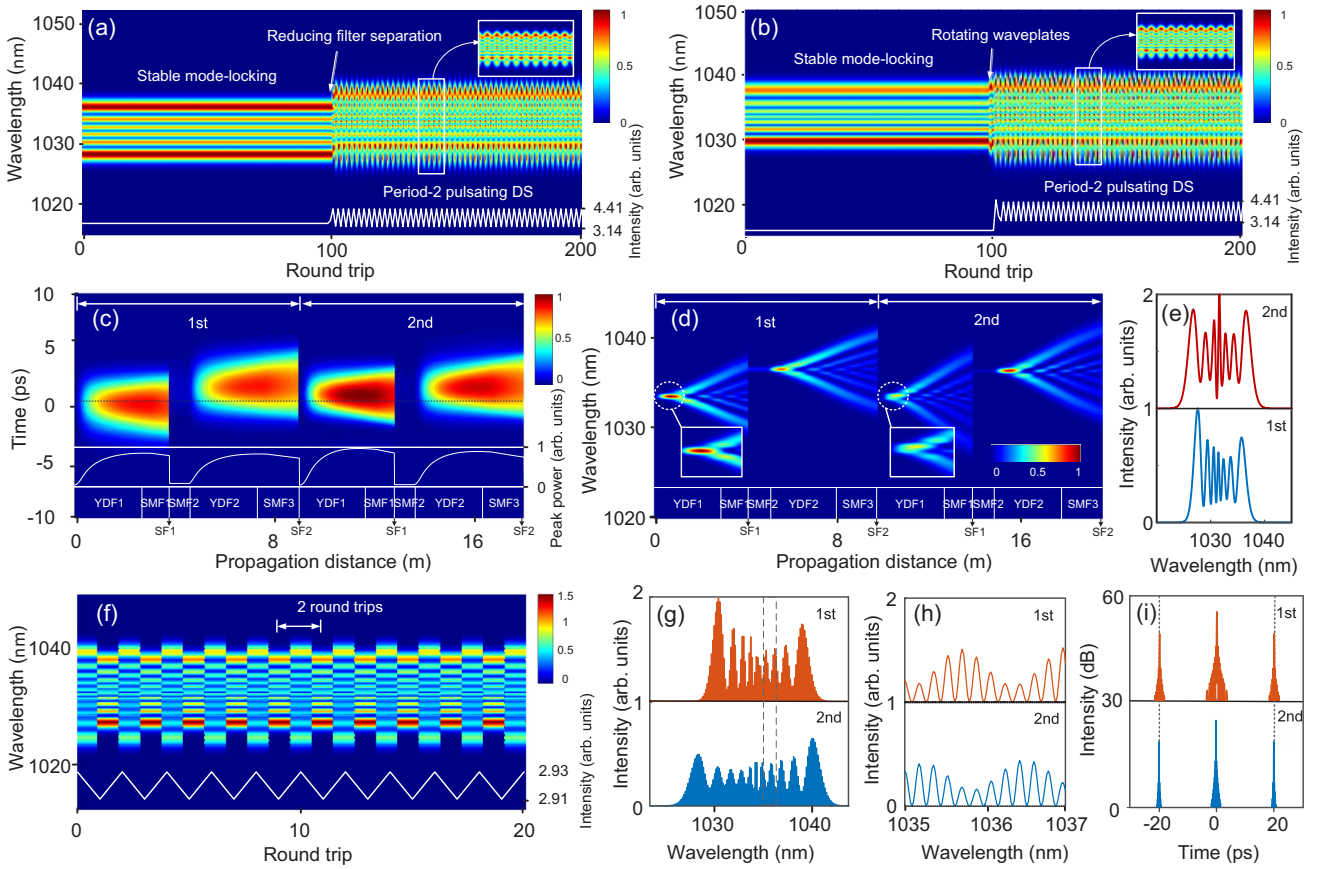

FIG. 5. Simulation of the pulsating DSs in a vector model. (a) Transition from stable mode-locking to pulsating DS by reducing the filter separation. (b) Transition into pulsation by rotating the wave plates. The white curves in panels (a) and (b) show the integrated spectral power change. (c) Temporal and (d) spectral dynamics within 2 successive round trips for a pulsation state. The white solid line in panel (c) is the peak power of the pulse in the cavity. The insets of panel (d) depict the zoom-in spectra right after filter 1 of 2 successive round trips. SF, spectral filter. (e) Normalized spectra before filter 2 in panel (d). (f) Evolution of spectrum of a DS molecule in period-2 pulsation. (g) Single-shot spectra of the period-2 pulsating bound soliton state in panel (f). (h) Zoom-in of the data in panel (g). (i) Fourier transform of panel (g) shows the pulse separation remains unchanged in pulsation.

TABLE I. Parameters of the optical fibers.

Fiber	Length (m)	β_2 (ps^2 km^{-1})	β_3 (ps^3 km^{-1})	γ (W^{-1} km^{-1})	L_B (m)	Gain bandwidth (nm)
YDF1	3.1	24.9	59	4.8	1	30
YDF2	3.1	24.9	59	4.8	1	30
SMF1	0.7	22.2	63.8	4.4	1	NA
SMF2	0.8	22.2	63.8	4.4	1	NA
SMF3	1.3	22.2	63.8	4.4	1	NA

TABLE II. Other parameters used in the simulations.

Figure	Filter separation (nm)	Filter bandwidth (nm)	g_0 (m^{-1})	E_{sat} (nJ)	ϕ_{QWP} (°)	ϕ_{HWP1} (°)
Fig. 5(a)	6 to 3	0.8	10	1	90	20
Fig. 5(b)	3	0.8	9	1	90 to 50	50
Fig. 5(c)	3	0.7	13	1.1	83	23
Fig. 5(f)	3	0.7	10	4	90	20
Fig. 6(a)	3	0.7	31.3	3.8	89.86	20
Fig. 6(e)	2.5	0.8	10	1	90	26
Fig. 6(g)	2.5	0.8	10	1	90	24
Fig. 7	2.5	1	10	1	NA	NA

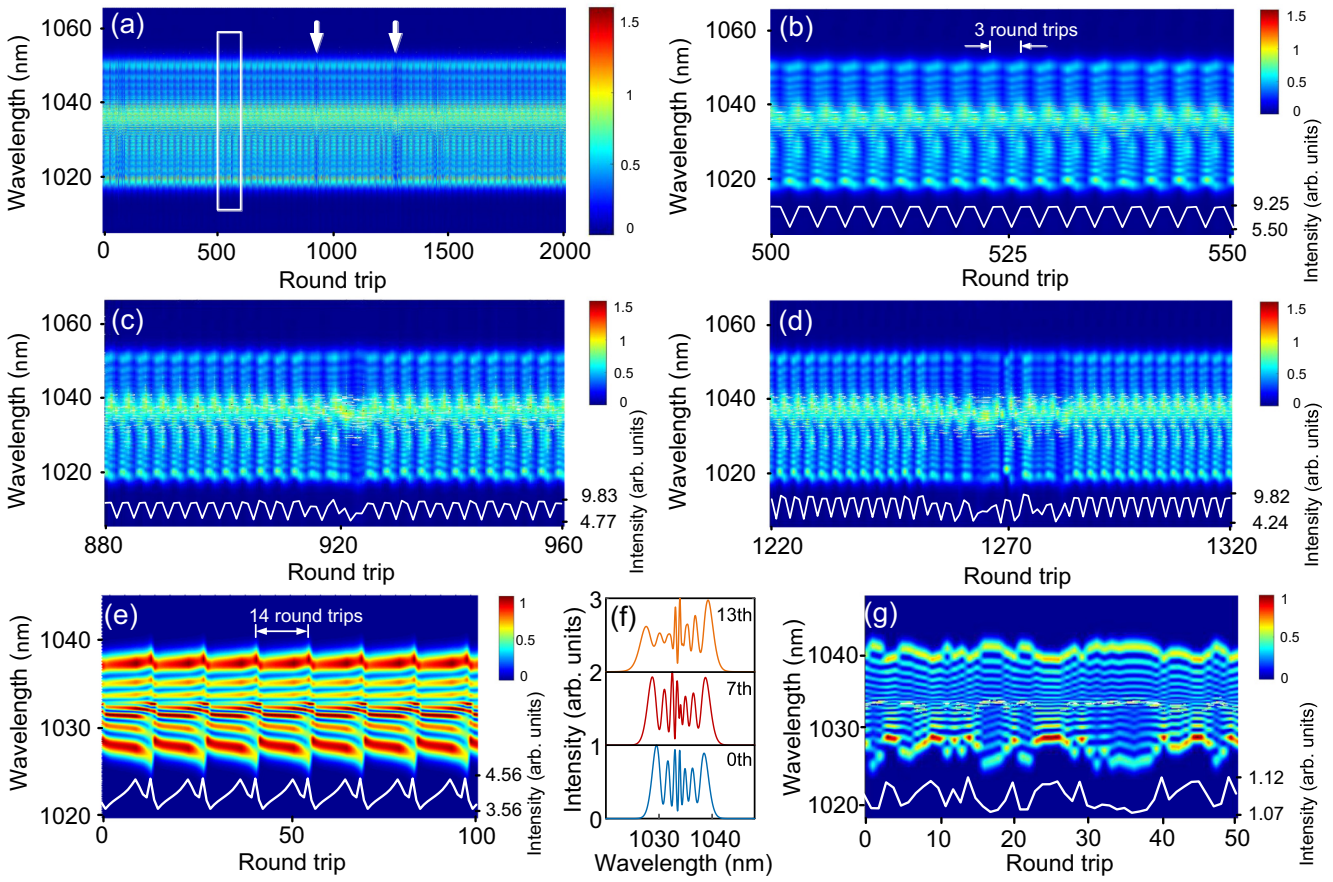

FIG. 6. Simulations of the pulsating soliton explosion and the long-period pulsation. (a) Evolution of the spectra in 2001 round trips in a period-3 pulsation with soliton explosion, marked by the arrows. (b) Zoom-in of the data marked by the rectangular shape in panel (a), showing regular period-3 pulsation. (c) and (d) Zoom-in of the data marked by the arrows in panel (a). (e) Evolution of the spectra of a long-period (period-14) pulsation state. (f) Three representative single-shot spectra within a pulsation period shown in panel (e). (g) Spectral evolution of a chaotic pulsation state which loses periodicity. The white curves in panels (b)–(d), (e), and (g) show the change of the integrated spectral power.

large pulse energy change in pulsation, as noted in Sec. III A. The intracavity pulse energy changes 1.3 times in the state of Fig. 5(c), which indicates that the intracavity energy also changes during pulsation. Furthermore, a typical pulsation state simulated using a scalar model only has a pulse energy change of ∼1.006 times (see the Appendix, Fig. 7). This further confirms that polarization dynamics is important to observe various pulsation dynamics in our MO. As an aside, the QWP can be rotated over 360° in some filter and pump power settings without losing mode-locking in simulations, which is also consistent with the observation noted in Sec. II.

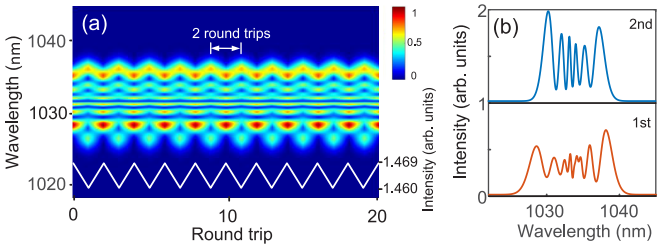

FIG. 7. Simulated pulsation in a scalar model. (a) Spectral dynamics for a period-2 pulsating DS. (b) Spectra for the pulsating DS in 2 successive round trips.

A pulsating DS molecule can also be simulated by injecting two separated weak pulses and increasing the gain saturation energy E_{sat} (corresponding to increasing the pump power in experiments, see Table II), as shown in Fig. 5(f). Single-shot spectra in 2 consecutive round trips [Fig. 5(g)] and their zoom-in views [Fig. 5(h)] show an change of spectral bandwidth as we observed in Fig. 2(i). Figure 5(i) is the Fourier transform of the simulated spectra, indicating that the pulse separation remains unchanged in this state, which agrees with the experiment.

B. Explosion and chaotic pulsation in simulations

Period-3 pulsation and DS explosion can also be attained by increasing the small signal gain g_0 as well as the saturation energy E_{sat} and finely tuning the wave plates (see the Appendix). Figures 6(a) and 6(b) show the spectral evolution over 2001 round trips and 51 round trips, respectively. Note that our simulation time window is limited to 100 ps (only one

DS is included in the window) so as to reduce the computation complexity. This simplification does not impact the pulsation dynamics significantly, since the interaction between two DSs in Fig. 3 is negligible. Similar to experimental observation, the simulated period-3 pulsation is associated with mild soliton explosion [indicated by arrows in Fig. 6(a)]. The zoom-in of the explosion is shown in Figs. 6(c) and 6(d). The spectrum transitions into a distorted one (around the 922nd round trip) and the pulse energy changes irregularly during the explosion [white line in Fig. 6(c)]. The DS recovers to the regular pulsation state after about 5 round trips. This explosion timescale is close to the measurements in Fig. 3. Figure 6(d) shows another example of soliton explosion during pulsation where the explosion lasts slightly longer (∼30 round trips). Note that the period-3 pulsation can be obtained under conditions similar to those used in Fig. 5, while the DS explosion can only be observed by increasing g_0 and E_{sat} to relatively large values (see Table II). Therefore, we believe that high pump power and strong nonlinearity are essential to the emergence of soliton explosions in MOs, which is consistent with the experimental observations. And it is in contrast to the explosion observed in Ref. [22], which occurs at a relatively low pump power.

Long-period and chaotic pulsation can also be simulated by rotating the wave plates (see the Appendix for used parameters). Figure 6(e) shows the spectral dynamics for a period-14 pulsation, while Fig. 6(f) shows three normalized representative spectra in a pulsation period [the 0th spectrum corresponds to the narrowest spectra in Fig. 6(e)]. Further rotation of the wave plates can generate chaotic pulsation as shown in Fig. 6(g). The corresponding pulse energy change loses periodicity. These simulations are in qualitative agreement with the observations in Fig. 4.

V. DISCUSSION AND CONCLUSION

Pulsation in concatenated Mamyshev regenerators was predicted to be initiated by varying the fiber dispersion parameters [36]. Here, we observe the pulsation by controlling the pump power, filter separation, or polarization dynamics, which are mainly nonlinear and dissipative effects. Since nonlinear gain/loss effects (e.g., quintic dissipative terms in CGLE) are essential for the generation of pulsation in mode-locked lasers [10], the saturable absorption based on the Mamyshev regenerator may provide these effects (slow gain dynamics are not included in our simulation). Instead of being monotonous with increasing pulse energy, the transmission curve of a Mamyshev generator can be oscillatory versus input energy [49] (see also Fig. 9 in the Appendix). The oscillatory transmission of a Mamyshev regenerator is equivalent to the overdriving of a saturable absorber and can be a possible reason leading to the observed pulsation [50,51].

In conclusion, we have experimentally and numerically observed pulsating DSs in a MO. These pulsating DSs arise under relatively high pump powers and small filter separation and bandwidths. We observe various pulsation dynamics for mode-locking states comprising a single DS or two DSs. By controlling the polarization state, dramatic pulse energy change up to as much as 40 times is possible. Soliton explosion during pulsation has also been observed in the MO under a relatively high pump power. The chaotic pulsation state also exists in the MO. Simulations are in qualitative agreement with the observations. Our results not only show that narrow filter separation should be avoided for stable operation of high power MOs but also add a different type of pulsating DS in optical systems. In addition to ultrafast laser systems, our work shows that too narrow filter separation and filter bandwidth should be avoid when using concatenated Mamyshev regenerators for optical signal processing and transmission.

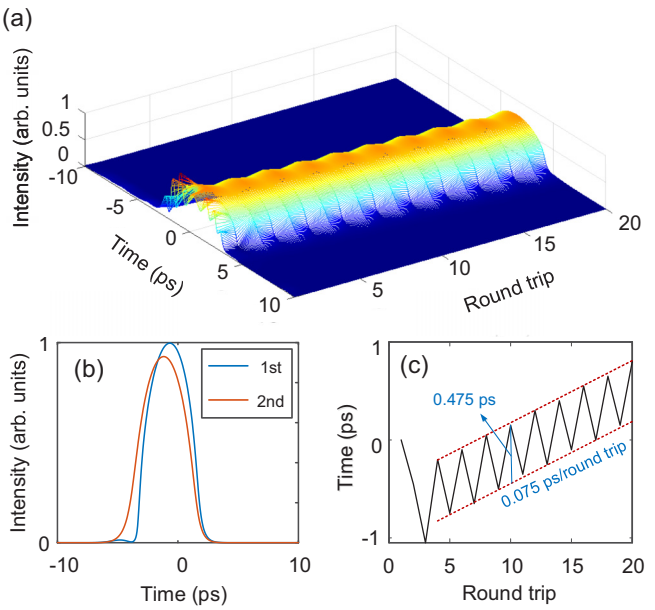

FIG. 8. Simulated temporal details in pulsation. (a) Spatiotemporal evolution for the period-2 pulsation state. (b) Zoom-in of 2 consecutive round trips. (c) Central position of the pulsating pulses in panel (a).

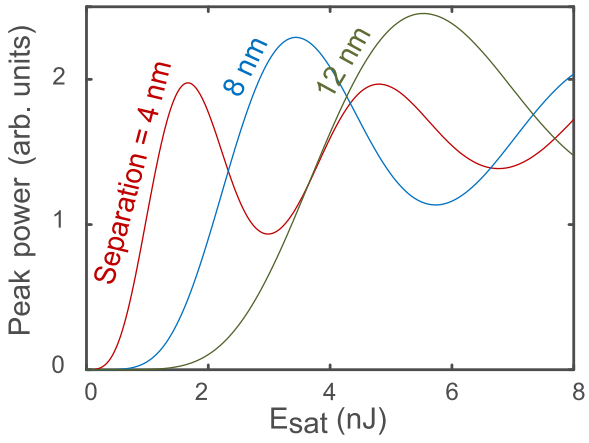

FIG. 9. Overdriving of a Mamyshev regenerator in the simulated MO. Transmitted pulse peak power from an offset filter under different filter separation. Filter bandwidth: 1 nm, $g_0 = 10\ \text{m}^{-1}$. Parameters of the input pulse: a Gaussian-shape pulse with a 3-dB bandwidth of 2 nm and a peak power of 50 W; the input pulse is centered at the first filter with a shorter wavelength and then filtered by the second filter with a longer wavelength.

ACKNOWLEDGMENTS

This work is supported by the National Natural Science Foundation of China (NSFC) (Grants No. 51527901 and No. 61575106), by the Tsinghua University Initiative Scientific Research Program, and by the fundamental Research Funds for the Central Universities (Grant No. BUPT 2021RC08).

The authors declare no conflicts of interest.

APPENDIX

1. Numerical simulation details

The simulation is based on a vector model where the pulse propagation is modeled as [52]

$$\frac{\partial u}{\partial z} = i\beta u - \delta\frac{\partial u}{\partial t} - \frac{i\beta_2}{2}\frac{\partial^2 u}{\partial t^2} + \frac{\beta_3}{6}\frac{\partial^3 u}{\partial t^3} + \frac{g}{2}u + \frac{g}{2\Omega_g^2}\frac{\partial^2 u}{\partial t^2} + i\gamma\left(|u|^2 + \frac{2}{3}|v|^2\right)u + \frac{i\gamma}{3}v^2u^*, \tag{A1}$$

$$\frac{\partial v}{\partial z} = -i\beta v + \delta\frac{\partial v}{\partial t} - \frac{i\beta_2}{2}\frac{\partial^2 v}{\partial t^2} + \frac{\beta_3}{6}\frac{\partial^3 v}{\partial t^3} + \frac{g}{2}v + \frac{g}{2\Omega_g^2}\frac{\partial^2 v}{\partial t^2} + i\gamma\left(|v|^2 + \frac{2}{3}|u|^2\right)v + \frac{i\gamma}{3}u^2v^*, \tag{A2}$$

where u and v are the slowly varying pulse envelopes of fast and slow axes of the cavity, respectively; and $2\beta = 2\pi/L_B$ and $\delta = d\beta/d\omega$ are the wave number difference and the inverse group velocity difference, respectively (L_B is the beat length and ω is the angular frequency). β_2 is the group velocity dispersion; γ is the Kerr nonlinearity coefficient; $g = g_0\exp[-\int(|u|^2 + |v|^2)dt/E_{\text{sat}}]$ is the saturated gain, with g_0 and E_{sat} being the small signal gain and the gain saturation energy, respectively; and Ω_g is the gain bandwidth. For passive fibers, small signal gain is chosen as $g_0 = 0\ \text{m}^{-1}$. The fiber parameters are fixed for all simulations (see Table I). Simulations start from two weak pulses along the fast and slow axes of the cavity (a weak pulse for the scalar model is discussed in Fig. 7) to speed up the convergence of our simulations. Starting from the Yb-doped gain fiber (YDF1), the weak pulses are amplified and experience spectral broadening due to SPM. The spectrum further broadens in the passive fiber (SMF1) before being filtered at both axes by filter 1 with a Gaussian profile. The filtered pulse experiences amplification and spectral broadening for the second time in SMF2, YDF2, and SMF3 [see Fig. 5(c) for the fiber order]. Then the pulse passes a QWP, a PBS, and two HWPs, which are modeled by the Jones matrices (angles are defined with respect to the x axis, which is assumed as one of fiber eigen-polarization axes). The PBS is inserted before the second HWP (HWP2) to select the x-polarized component as the output. Finally, the pulse is filtered by filter 2, whose transmission window is shifted to longer wavelengths from filter 1. Then the loop is closed. HWP2 is fixed to have an orientation of 90°. The parameters used to generate the various pulsation dynamics are listed in Table II.

The parameters used in the simulations are in reasonable agreement with experimental measurements. Some conditions may differ from the experiments; for example, the active fibers in two arms share the same gain parameters (g_0 and E_{sat}) and the filter properties (bandwidth and separation) are adjusted in simulations (fixed in experiments). These slight discrepancies arise from the difficulty in modeling the complex MO accurately and the need to reduce the parameter space to explore and computation complexity. However, the discrepancies will not cause the loss of generality. For example, the simulated pulsating DS and other results we discussed above can be attained under different lengths of YDF and SMF by adjusting g_0 and E_{sat} as well as the filter parameters.

We also use a scale model similar to Ref. [53] to verify the existence of pulsation in MOs. We neglect the polarization effect of all components and get the output from a linear output port with a coupling ratio of 20% after the SMF2. Figure 7(a) shows a typical pulsation state simulated using the scalar model, which only has a pulse energy change of ∼1.006 times. Figure 7(b) plots the pulsating spectra for 2 successive round trips, showing the variation of both the spectral shape and the bandwidth.

2. Spatiotemporal dynamics

Figure 8(a) shows the spatiotemporal evolution of the period-2 pulsating soliton over 21 round trips. Both the intensity and the profile of the pulses change slightly during pulsation, as shown in Fig. 8(b). In addition, the center position of the pulse is plotted in Fig. 8(c), which shows a change of 0.475 ps for the pulse position in each pulsating period. The red dashed lines shows the pulse center position has an overall motion of 0.075 ps per round trip.

3. Mamyshev regenerator transmittance curve

Similar to other materials-based or artificial saturable absorbers, Mamyshev regenerators feature also an overdriving characteristic [25,49]. In other words, its transmittance is oscillatory at high input pulse power [25,49]. Such oscillatory transmission can be more significant when the spectral broadening is SPM-dominated and features spectral fringes [see Fig. 5(e) and Fig. 7(b)]. In this case, the regenerator can experience high (low) transmission when the passband of the filter overlaps with the peak (valley) of the fringes, assuming the filter bandwidth is not much larger than the fringe spacings. Since the positions of spectral fringe peaks and valleys depend upon pulse peak power, the transmission exhibits an oscillatory curve (i.e., overdriving) for fixed filter positions. We simulate the transmission curve by passing a narrow-band pulse through a 3.1-m ytterbium-doped fiber and calculating its peak power after being filtered by an offset Gaussian filter (simulation conditions are listed in the caption to Fig. 9). The transmission curve exhibits the overdriving feature under different gain saturation energies E_{sat} (see Fig. 9).

The central fringe occurs first when increasing pulse peak power in SPM-based spectral broadening. Hence, when the filter separation is narrower, the MO needs a lower E_{sat} to have overdriving of the regenerator in simulations (see Fig. 9). The simulated overdriving can be a possible reason for the observed pulsation in the main text and this can be the reason that pulsation arises more frequently with a narrow filter separation.

[1] N. Akhmediev and A. Ankiewicz (Eds.), *Dissipative Solitons: From Optics to Biology and Medicine*, Lecture Notes in Physics Vol. 751 (Springer-Verlag, Berlin, 2008).

[2] C. Xu and F. Wise, Recent advances in fibre lasers for nonlinear microscopy, Nat. Photonics **7**, 875 (2013).

[3] J. Kim and F. X. Kärtner, Attosecond-precision ultrafast photonics, Laser Photonics Rev. **4**, 432 (2010).

[4] T. J. Kippenberg, A. L. Gaeta, M. Lipson, and M. L. Gorodetsky, Dissipative Kerr solitons in optical microresonators, Science **361**, eaan8083 (2018).

[5] N. Akhmediev and V. Korneev, Modulation instability and periodic solutions of the nonlinear Schrödinger equation, Theor. Math. Phys. **69**, 1089 (1986).

[6] J. M. Dudley, F. Dias, M. Erkintalo, and G. Genty, Instabilities, breathers and rogue waves in optics, Nat. Photonics **8**, 755 (2014).

[7] P. Grelu and N. Akhmediev, Dissipative solitons for mode-locked lasers, Nat. Photonics **6**, 84 (2012).

[8] R. J. Deissler and H. R. Brand, Periodic, Quasiperiodic, and Chaotic Localized Solutions of the Quintic Complex Ginzburg-Landau Equation, Phys. Rev. Lett. **72**, 478 (1994).

[9] J. M. Soto-Crespo, N. Akhmediev, and A. Ankiewicz, Pulsating, Creeping, and Erupting Solitons in Dissipative Systems, Phys. Rev. Lett. **85**, 2937 (2000).

[10] N. Akhmediev, J. M. Soto-Crespo, and G. Town, Pulsating solitons, chaotic solitons, period doubling, and pulse coexistence in mode-locked lasers: Complex Ginzburg-Landau equation approach, Phys. Rev. E **63**, 056602 (2001).

[11] K. M. Spaulding, D. H. Yong, A. D. Kim, and J. N. Kutz, Nonlinear dynamics of mode-locking optical fiber ring lasers, J. Opt. Soc. Am. B **19**, 1045 (2002).

[12] A. B. Matsko, A. A. Savchenkov, and L. Maleki, On excitation of breather solitons in an optical microresonator, Opt. Lett. **37**, 4856 (2012).

[13] C. Bao, J. A. Jaramillo-Villegas, Y. Xuan, D. E. Leaird, M. Qi, and A. M. Weiner, Observation of Fermi-Pasta-Ulam Recurrence Induced by Breather Solitons in an Optical Microresonator, Phys. Rev. Lett. **117**, 163901 (2016).

[14] J. M. Soto-Crespo, M. Grapinet, P. Grelu, and N. Akhmediev, Bifurcations and multiple-period soliton pulsations in a passively mode-locked fiber laser, Phys. Rev. E **70**, 066612 (2004).

[15] L. Zhao, D. Tang, F. Lin, and B. Zhao, Observation of period-doubling bifurcations in a femtosecond fiber soliton laser with dispersion management cavity, Opt. Express **12**, 4573 (2004).

[16] B. Zhao, D. Y. Tang, L. M. Zhao, P. Shum, and H. Y. Tam, Pulse-train nonuniformity in a fiber soliton ring laser mode-locked by using the nonlinear polarization rotation technique, Phys. Rev. A **69**, 043808 (2004).

[17] P. Wang, X. Xiao, P. Grelu, and C. Yang, Subsideband generation associated with period-N pulsations in Tm soliton fiber lasers, IEEE Photonics J. **9**, 1 (2017).

[18] K. Goda and B. Jalali, Dispersive Fourier transformation for fast continuous single-shot measurements, Nat. Photonics **7**, 102 (2013).

[19] M. Liu, Z.-W. Wei, H. Li, T.-J. Li, A.-P. Luo, W.-C. Xu, and Z.-C. Luo, Visualizing the invisible soliton pulsation in an ultrafast laser, Laser Photonics Rev. **14**, 1900317 (2020).

[20] H.-J. Chen, Y.-J. Tan, J.-G. Long, W.-C. Chen, W.-Y. Hong, H. Cui, A.-P. Luo, Z.-C. Luo, and W.-C. Xu, Dynamical diversity of pulsating solitons in a fiber laser, Opt. Express **27**, 28507 (2019).

[21] J. Peng, S. Boscolo, Z. Zhao, and H. Zeng, Breathing dissipative solitons in mode-locked fiber lasers, Sci. Adv. **5**, eaax1110 (2019).

[22] J. Peng and H. Zeng, Experimental Observations of Breathing Dissipative Soliton Explosions, Phys. Rev. Applied **12**, 034052 (2019).

[23] Y. Cui, Y. Zhang, Y. Song, L. Huang, L. Tong, J. Qiu, and X. Liu, XPM-induced vector asymmetrical soliton with spectral period doubling in mode-locked fiber laser, Laser Photonics Rev. **15**, 2000216 (2021).

[24] Z. Wang, Z. Wang, Y. Liu, R. He, J. Zhao, G. Wang, and G. Yang, Self-organized compound pattern and pulsation of dissipative solitons in a passively mode-locked fiber laser, Opt. Lett. **43**, 478 (2018).

[25] P. Mamyshev, All-optical data regeneration based on self-phase modulation effect, in *24th European Conference on Optical Communication, Madrid, Spain* (IEEE, New York, 1998), Vol. 1, pp. 475–476.

[26] K. Regelskis, J. Želudevičius, K. Viskontas, and G. Račiukaitis, Ytterbium-doped fiber ultrashort pulse generator based on self-phase modulation and alternating spectral filtering, Opt. Lett. **40**, 5255 (2015).

[27] Z. Liu, Z. M. Ziegler, L. G. Wright, and F. W. Wise, Megawatt peak power from a Mamyshev oscillator, Optica **4**, 649 (2017).

[28] P. Sidorenko, W. Fu, L. G. Wright, M. Olivier, and F. W. Wise, Self-seeded, multi-megawatt, Mamyshev oscillator, Opt. Lett. **43**, 2672 (2018).

[29] W. Liu, R. Liao, J. Zhao, J. Cui, Y. Song, C. Wang, and M. Hu, Femtosecond Mamyshev oscillator with 10-MW-level peak power, Optica **6**, 194 (2019).

[30] P. Repgen, B. Schuhbauer, M. Hinkelmann, D. Wandt, A. Wienke, U. Morgner, J. Neumann, and D. Kracht, Mode-locked pulses from a thulium-doped fiber Mamyshev oscillator, Opt. Express **28**, 13837 (2020).

[31] V. Boulanger, M. Olivier, F. Guilbert-Savary, F. Trépanier, M. Bernier, and M. Piché, All-fiber Mamyshev oscillator enabled by chirped fiber Bragg gratings, Opt. Lett. **45**, 3317 (2020).

[32] M. Rochette, L. R. Chen, K. Sun, and J. Hernandez-Cordero, Multiwavelength and tunable self-pulsating fiber cavity based on regenerative SPM spectral broadening and filtering, IEEE Photonics Technol. Lett. **20**, 1497 (2008).

[33] S. Pitois, C. Finot, L. Provost, and D. J. Richardson, Generation of localized pulses from incoherent wave in optical fiber lines made of concatenated Mamyshev regenerators, J. Opt. Soc. Am. B **25**, 1537 (2008).

[34] T. North and M. Rochette, Regenerative self-pulsating sources of large bandwidths, Opt. Lett. **39**, 174 (2014).

[35] C. Ma, A. Khanolkar, Y. Zang, and A. Chong, Ultrabroadband, few-cycle pulses directly from a Mamyshev fiber oscillator, Photonics Res. **8**, 65 (2020).

[36] S. Pitois, C. Finot, and L. Provost, Asymptotic properties of incoherent waves propagating in an all-optical regenerators line, Opt. Lett. **32**, 3263 (2007).

[37] S. T. Cundiff, J. M. Soto-Crespo, and N. Akhmediev, Experimental Evidence for Soliton Explosions, Phys. Rev. Lett. **88**, 073903 (2002).

[38] A. F. Runge, N. G. Broderick, and M. Erkintalo, Observation of soliton explosions in a passively mode-locked fiber laser, Optica **2**, 36 (2015).

[39] Y. Zhou, Y.-X. Ren, J. Shi, and K. K. Wong, Breathing dissipative soliton explosions in a bidirectional ultrafast fiber laser, Photonics Res. **8**, 1566 (2020).

[40] A. Chong, J. Buckley, W. Renninger, and F. W. Wise, All-normal-dispersion femtosecond fiber laser, Opt. Express **14**, 10095 (2006).

[41] Y.-H. Chen, P. Sidorenko, R. Thorne, and F. Wise, Starting dynamics of a linear-cavity femtosecond Mamyshev oscillator, J. Opt. Soc. Am. B **38**, 743 (2021).

[42] P. Grelu, J. Béal, and J. Soto-Crespo, Soliton pairs in a fiber laser: from anomalous to normal average dispersion regime, Opt. Express **11**, 2238 (2003).

[43] W. Chang, J. M. Soto-Crespo, P. Vouzas, and N. Akhmediev, Extreme soliton pulsations in dissipative systems, Phys. Rev. E **92**, 022926 (2015).

[44] J. Peng, Z. Zhao, S. Boscolo, C. Finot, S. Sugavanam, D. V. Churkin, and H. Zeng, Breather molecular complexes in a passively mode-locked fiber laser, Laser Photonics Rev. **15**, 2000132 (2021).

[45] L. Gui, P. Wang, Y. Ding, K. Zhao, C. Bao, X. Xiao, and C. Yang, Soliton molecules and multisoliton states in ultrafast fibre lasers: Intrinsic complexes in dissipative systems, Appl. Sci. **8**, 201 (2018).

[46] G. Herink, F. Kurtz, B. Jalali, D. R. Solli, and C. Ropers, Real-time spectral interferometry probes the internal dynamics of femtosecond soliton molecules, Science **356**, 50 (2017).

[47] K. Krupa, K. Nithyanandan, U. Andral, P. Tchofo-Dinda, and P. Grelu, Real-Time Observation of Internal Motion within Ultrafast Dissipative Optical Soliton Molecules, Phys. Rev. Lett. **118**, 243901 (2017).

[48] X. Liu, X. Yao, and Y. Cui, Real-Time Observation of the Buildup of Soliton Molecules, Phys. Rev. Lett. **121**, 023905 (2018).

[49] L. Provost, C. Finot, P. Petropoulos, K. Mukasa, and D. J. Richardson, Design scaling rules for 2R-optical self-phase modulation-based regenerators, Opt. Express **15**, 5100 (2007).

[50] F. Li, P. K. A. Wai, and J. N. Kutz, Geometrical description of the onset of multi-pulsing in mode-locked laser cavities, J. Opt. Soc. Am. B **27**, 2068 (2010).

[51] L. Kong, X. Xiao, and C. Yang, Operating regime analysis of a mode-locking fiber laser using a difference equation model, J. Opt. **13**, 105201 (2011).

[52] D. Y. Tang, H. Zhang, L. M. Zhao, and X. Wu, Observation of High-Order Polarization-Locked Vector Solitons in a Fiber Laser, Phys. Rev. Lett. **101**, 153904 (2008).

[53] P. Wang, S. Yao, P. Grelu, X. Xiao, and C. Yang, Pattern formation in 2-μm Tm Mamyshev oscillators associated with the dissipative Faraday instability, Photonics Res. **7**, 1287 (2019).